


RESEARCH

Open Access



Redesigning N-glycosylation sites in a GH3 β -xylosidase improves the enzymatic efficiency

Marcelo Ventura Rubio¹, César Rafael Fanchini Terrasan¹, Fabiano Jares Contesini¹, Mariane Paludetti Zubieta¹, Jaqueline Aline Gerhardt¹, Leandro Cristante Oliveira², Any Elisa de Souza Schmidt Gonçalves³, Fausto Almeida⁴, Bradley Joseph Smith¹, Gustavo Henrique Martins Ferreira de Souza¹, Artur Hernando Sampaio Dias⁵, Munir Skaf⁵ and André Damasio^{1*} 

Abstract

Background: β -Xylosidases are glycoside hydrolases (GHs) that cleave xylooligosaccharides and/or xylobiose into shorter oligosaccharides and xylose. *Aspergillus nidulans* is an established genetic model and good source of carbohydrate-active enzymes (CAZymes). Most fungal enzymes are N-glycosylated, which influences their secretion, stability, activity, signalization, and protease protection. A greater understanding of the N-glycosylation process would contribute to better address the current bottlenecks in obtaining high secretion yields of fungal proteins for industrial applications.

Results: In this study, BxIB—a highly secreted GH3 β -xylosidase from *A. nidulans*, presenting high activity and several N-glycosylation sites—was selected for N-glycosylation engineering. Several glycomutants were designed to investigate the influence of N-glycans on BxIB secretion and function. The non-glycosylated mutant (BxIB^{non-glyc}) showed similar levels of enzyme secretion and activity compared to the wild-type (BxIB^{wt}), while a partially glycosylated mutant (BxIB^{N1;5;7}) exhibited increased activity. Additionally, there was no enzyme secretion in the mutant in which the N-glycosylation context was changed by the introduction of four new N-glycosylation sites (BxIB^{CC}), despite the high transcript levels. BxIB^{wt}, BxIB^{non-glyc}, and BxIB^{N1;5;7} formed similar secondary structures, though the mutants had lower melting temperatures compared to the wild type. Six additional glycomutants were designed based on BxIB^{N1;5;7}, to better understand its increased activity. Among them, the two glycomutants which maintained only two N-glycosylation sites each (BxIB^{N1;5} and BxIB^{N5;7}) showed improved catalytic efficiency, whereas the other four mutants' catalytic efficiencies were reduced. The N-glycosylation site N5 is important for improved BxIB catalytic efficiency, but needs to be complemented by N1 and/or N7. Molecular dynamics simulations of BxIB^{non-glyc} and BxIB^{N1;5} reveals that the mobility pattern of structural elements in the vicinity of the catalytic pocket changes upon N1 and N5 N-glycosylation sites, enhancing substrate binding properties which may underlie the observed differences in catalytic efficiency between BxIB^{non-glyc} and BxIB^{N1;5}.

Conclusions: This study demonstrates the influence of N-glycosylation on *A. nidulans* BxIB production and function, reinforcing that protein glycoengineering is a promising tool for enhancing thermal stability, secretion, and enzymatic activity. Our report may also support biotechnological applications for N-glycosylation modification of other CAZymes.

Keywords: β -Xylosidase, *Aspergillus nidulans*, N-glycosylation, Enzyme secretion, Glycomutants, CAZyme, Glycoside hydrolase family 3

*Correspondence: adamasio@unicamp.br

¹ Department of Biochemistry and Tissue Biology, Institute of Biology, University of Campinas (UNICAMP), Rua Monteiro Lobato, 255, Cidade Universitária Zeferino Vaz, Campinas, SP 13083-862, Brazil

Full list of author information is available at the end of the article



Background

Filamentous fungi possess several genes related to plant biomass degradation, which makes them important sources of CAZymes with high enzyme secretion capabilities [1]. However, enzyme yield is a significant bottleneck in economically feasible production of plant cell wall-degrading enzymes. Glycoside hydrolase family 3 (GH3) enzymes produced by *Aspergillus* spp.—such as β -xylosidase, β -glucosidase, α -L-arabinofuranosidase, and exo-1,3-1,4- β -glucanase—are important enzymes with diverse activities. GH3 enzymes with β -xylosidase activity (xylan 1,4- β -D-xylosidase, EC 3.2.1.37) perform hemicellulose degradation by hydrolyzing non-reducing ends of xylooligosaccharides and/or xylobiose, releasing xylose. These enzymes play a central role in plant biomass degradation, having applications in biofuel, paper, food, and animal feed industries [2].

Several post-translational modifications (PTMs) occur on microbial proteins, including those in bacteria and fungi. N-glycosylation is one of the most important PTMs—influencing protein secretion, stability, activity, signalization, and protease protection [3]. In addition, many proteins produced by filamentous fungi are N-glycosylated, including those generated and secreted by *Aspergillus nidulans* [4]. N-glycosylation is catalyzed by oligosaccharyltransferases in the lumen of the endoplasmic reticulum (ER), and involves the attachment of a glycan to an asparagine (N) residue; it is found in 70% of predicted N-glycosylation consensus sequences or sequons (N-X-S/T, where X is any amino acid except proline, and S/T is serine or threonine) [5].

The influence of N-glycans on CAZyme properties can be exemplified with several proteins. For example, a thermophilic GH10 xylanase from *Aspergillus fumigatus* expressed in *Pichia pastoris* has improved activity and thermal stability in the N-glycosylated form, in comparison with the non-glycosylated form [6]. In another example, the position of N-linked glycans can positively or negatively influence the processivity of a GH6 cellobiohydrolase from *Penicillium verruculosum* [7]. Moreover, engineered N-glycosylation sites were shown to improve the thermal stability of cutinase C from *Aspergillus oryzae* by inhibiting thermal aggregation [8].

Aspergillus nidulans is a model organism for studying the secretion of recombinant enzymes [9–11]. However, studies investigating the role of N-glycosylation in enzyme secretion by filamentous fungi are scarce [12–15]. A recent study used N-glycoproteomics and N-glycomics to determine N-glycosylation patterns of proteins secreted from *A. nidulans* grown in glucose, xylan, and NaOH-pretreated sugarcane bagasse. More than 50% of the 265 identified N-glycoproteins were classified as CAZymes [4]. Among them, some industrially relevant

enzymes were highly secreted, making them relevant targets for investigating the influence of N-glycosylation on enzymatic properties and secretion. Here, a GH3 (BxlB^{wt}) secreted by *A. nidulans* A773 with high activity toward ρ -nitrophenyl- β -D-xylopyranoside (ρ NP-X), was selected as a model for N-glycosylation engineering. BxlB^{wt} harbors seven putative N-glycosylation sites validated by LC-MS/MS. Site-directed mutagenesis was used to produce BxlB glycomutants exhibiting different N-glycosylation profiles, which were then used to investigate whether the absence or addition of specific N-glycosylation sites would influence enzyme production, secretion, kinetics, and stability. We observed two N-glycosylation sites that were important for BxlB catalytic efficiency. In addition, we observed that BxlB synthesis may be completely compromised by changing the N-glycosylation context.

Results

BxlB^{wt} has seven predicted N-glycosylation sites

BxlB^{wt} is one of the five most secreted enzymes by *A. nidulans* when cultivated on different polymeric substrates, and is the most secreted hemicellulase during cultivation on beechwood xylan [4]. BxlB^{wt} is a highly N-glycosylated enzyme belonging to the GH3 family, presenting seven predicted N-glycosylation sites (NetNGlyc 1.0 Server)—all of them were validated by mass spectrometry: N63, N340, N408, N458, N419, N621 and N760.

N-glycosylation sequons were mutated by replacing asparagine (N) with glutamine (Q) and three BxlB glycomutants were designed: BxlB^{non-glyc}, a non-glycosylated variant in which all N-glycosylation sites were mutated; BxlB^{N1;5;7}, a partially glycosylated variant in which N340, N408, N419, and N621 were mutated; and BxlB^{CC}, a variant in which four new N-glycosylation sites were added using BxlB^{non-glyc} as template. The design of the new sites was based on the homology with 33 β -xylosidases sequences from aspergilli (Additional file 1: Figure S1). In addition, the accessible surface area (ASA) for each new N-glycosylation site was calculated (Fig. 1 and Additional file 1: Table S1). The design of BxlB^{CC} enabled the explicit verification of the importance of N-glycosylation position for β -xylosidase production, secretion, and function.

Production of BxlB glycomutants in *A. nidulans*

All *bxlB* gene variants were cloned into the pEXPYR vector controlled by the *glaA* promoter and the glucosylase signal peptide (SP) from *A. niger*, and then transformed into the *A. nidulans* A773 parental strain, before being cultivated with the inducer maltose [11]. Analyses of crude supernatants revealed that the non-glycosylated mutant (BxlB^{non-glyc}) presented similar levels of activity to the wild type (Fig. 2), while the BxlB^{N1;5;7} mutant showed 1.5-fold higher enzymatic activity. Although BxlB^{CC}

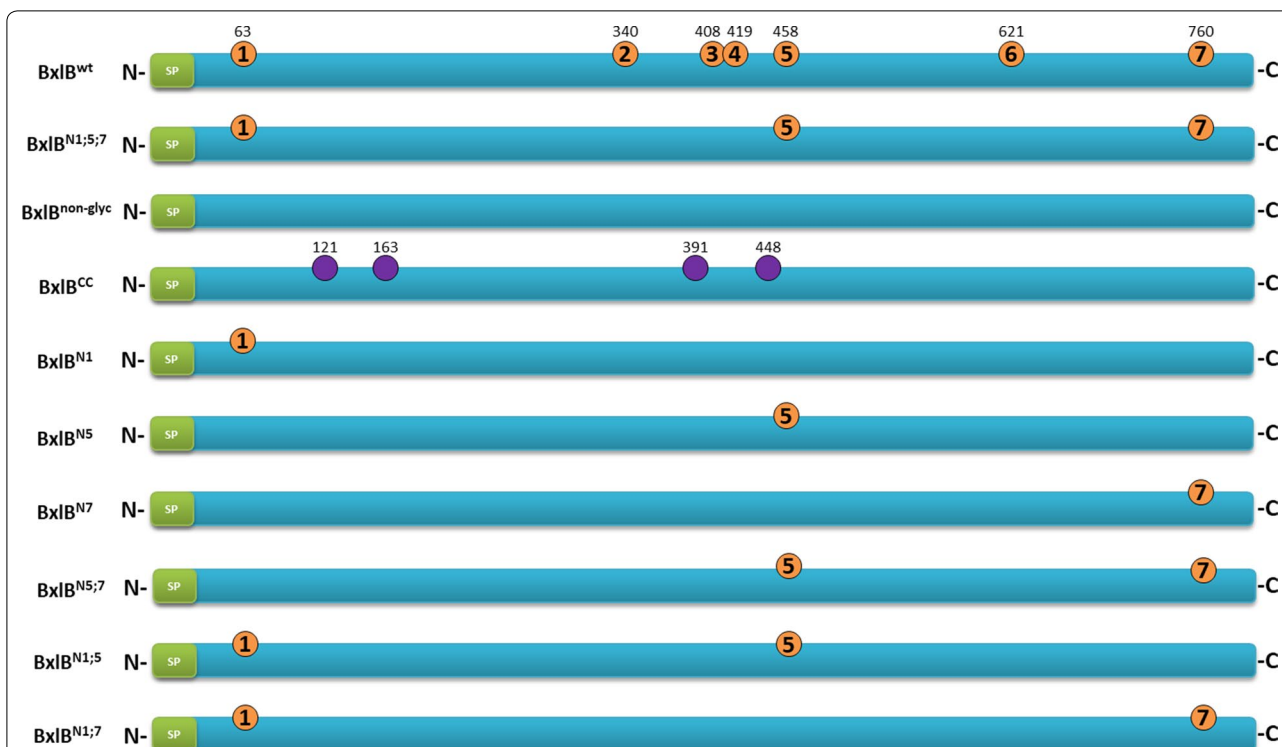


Fig. 1 Overview of BxlB glycomutants. BxlB^{wt} N-glycosylation sites were predicted by the NetNGlyc server, and all of these sites were validated by LC-MS/MS (orange circles). Three glycomutants were synthesized: BxlB^{N1;5;7}, N-to-Q mutation of four validated N-glycosylated sites; BxlB^{non-glyc}, N-to-Q mutation of the seven predicted N-glycosylation sites; BxlB^{CC}, addition of four new sites using BxlB^{non-glyc} as a template, to change the N-glycosylation context, N121 (A123T), Q166 N, Q391 N, and N448 (L450T). Six additional mutants were designed by using the BxlB^{non-glyc} as a template maintaining individual N-glycosylation sites (BxlB^{N1}, BxlB^{N5}, BxlB^{N7}) or combining two sites (BxlB^{N1;5}, BxlB^{N5;7}, BxlB^{N1;7}). SP: signal peptide, N: amino-terminus, C: carboxy-terminus

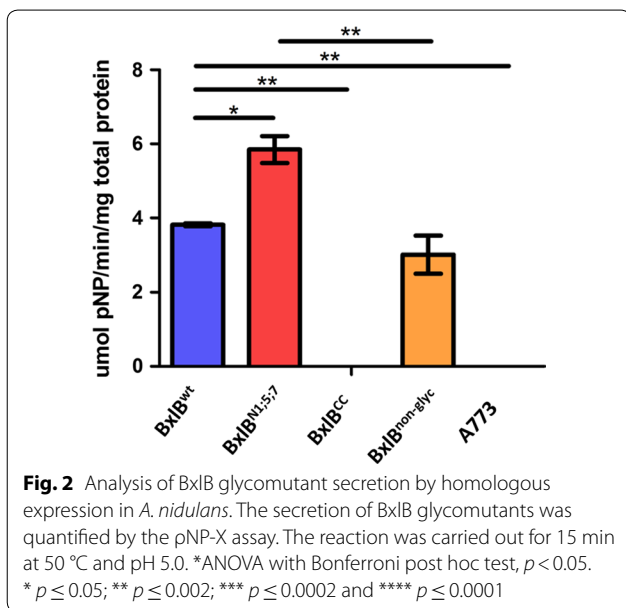


Fig. 2 Analysis of BxlB glycomutant secretion by homologous expression in *A. nidulans*. The secretion of BxlB glycomutants was quantified by the pNP-X assay. The reaction was carried out for 15 min at 50 °C and pH 5.0. *ANOVA with Bonferroni post hoc test, $p < 0.05$. * $p \leq 0.05$; ** $p \leq 0.002$; *** $p \leq 0.0002$ and **** $p \leq 0.0001$

activity could not be detected, the identification of some peptides was verified by mass spectrometry (Additional file 1: Table S2).

In addition, very low BxlB^{CC} intracellular activity was detected (similar to the parental strain) (Additional file 1: Figure S2), and intermediate activity levels were found for BxlB^{wt} and BxlB^{non-glyc}. BxlB^{N1;5;7}, in turn, presented fourfold higher intracellular activity in relation to BxlB^{wt}. Real-time PCR revealed that all BxlB glycomutants were properly transcribed, and no direct relationship between gene expression and enzyme production could be observed (Additional file 1: Figure S3).

Understanding the BxlB^{N1;5;7} higher catalytic efficiency

Enzymatic activity was measured at pH 5.0 and 60 °C for all the BxlB glycomutants and the wild type. K_m values for BxlB^{wt}, BxlB^{N1;5;7}, and BxlB^{non-glyc} were 2.06, 2.49, and 2.36 mM, respectively, while corresponding V_{max}

Table 1 Overview of kinetic parameters of BxlB glycomutants

	K_m (mM)	V_{max} (U/mg)	k_{cat} (1/s)	k_{cat}/K_m	k_{cat}/K_m (%) ^a
BxlB ^{wt}	2.06 ± 0.13	9.55 ± 0.18	13.08	6.34	100
BxlB ^{N1;5;7}	2.49 ± 0.43	17.28 ± 1.07	23.67	9.51	150
BxlB ^{non-glyc}	2.36 ± 0.11	10.12 ± 0.14	13.86	5.87	93
BxlB ^{N1}	2.53 ± 0.23	9.49 ± 0.28	13.01	5.13	81
BxlB ^{N5}	2.71 ± 0.21	6.08 ± 0.16	3.71	0.61	10
BxlB ^{N7}	3.19 ± 0.22	3.42 ± 0.09	4.37	1.27	20
BxlB ^{N5;7}	2.81 ± 0.11	20.47 ± 0.28	28.04	9.94	157
BxlB ^{N1;5}	2.91 ± 0.18	21.95 ± 0.51	30.07	10.33	163
BxlB ^{N1;7}	9.92 ± 1.05	4.12 ± 0.26	5.64	0.57	9

^a Relative to BxlB^{wt}

values were 9.55, 17.28, and 10.12 U/mg prot. Thus, the BxlB^{N1;5;7} glycomutant showed 50% higher catalytic efficiency as compared to the wild type, while BxlB^{non-glyc} catalytic efficiency was reduced by 7% (Table 1).

To better understand the improvement of the BxlB^{N1;5;7} catalytic efficiency, six additional glycomutants were designed by maintaining the following N-glycosylation sites: N1 (BxlB^{N1}), N5 (BxlB^{N5}), N7 (BxlB^{N7}), both N5 and N7 (BxlB^{N5;7}), both N1 and N5 (BxlB^{N1;5}), and both N1 and N7 (BxlB^{N1;7}) (Fig. 1). The genes encoding these proteins were also cloned into the pEXPYR vector and transformed into *A. nidulans* A773.

Analysis of kinetic parameters showed that, in comparison to the wild type, BxlB^{N5}, BxlB^{N7} and BxlB^{N1;7} catalytic efficiencies were drastically reduced, and BxlB^{N1} catalytic efficiency was partially reduced. BxlB^{N1;5} and BxlB^{N5;7} displayed the highest catalytic efficiencies with increases of 63% and 57%, respectively (Table 1).

To investigate how the N-glycosylation might affect the overall flexibility of the enzyme, we performed molecular dynamics (MD) atomistic simulations of both BxlB^{N1;5} and BxlB^{non-glyc} and computed the RMSF for each residue relative to the average structures (Fig. 3a). The presence of glycans at N1 and N5 increases the overall flexibility of the protein, especially in major segments that surround the catalytic site, but promotes stabilization of some structural elements of the enzyme (Fig. 3b).

The BxlB^{N1;5} catalytic site is more stable than in BxlB^{non-glyc}

The stability of the catalytic site in each system was examined by computing the distances between the α -carbons of the two catalytic residues—Asp288 and Glu491—along the molecular trajectories of both simulations. The average distances were 16.1 ± 1.6 Å and 18.4 ± 2.4 Å for the BxlB^{N1;5} and BxlB^{non-glyc} models, respectively, with a slightly narrower distribution for BxlB^{N1;5} (Fig. 4). The

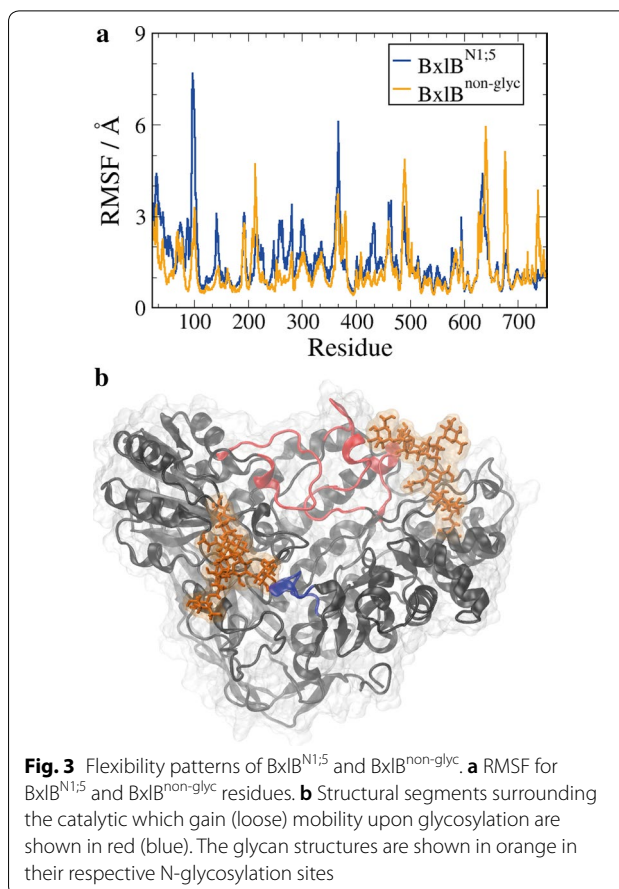


Fig. 3 Flexibility patterns of BxlB^{N1;5} and BxlB^{non-glyc}. **a** RMSF for BxlB^{N1;5} and BxlB^{non-glyc} residues. **b** Structural segments surrounding the catalytic which gain (loose) mobility upon glycosylation are shown in red (blue). The glycan structures are shown in orange in their respective N-glycosylation sites

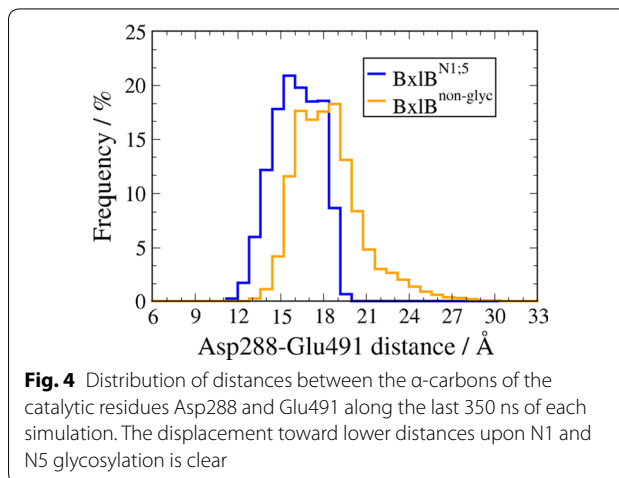


Fig. 4 Distribution of distances between the α -carbons of the catalytic residues Asp288 and Glu491 along the last 350 ns of each simulation. The displacement toward lower distances upon N1 and N5 glycosylation is clear

average distance between the corresponding Asp/Glu residues in other GH3 members, as measured from the crystal structures in PDB: 1IEX [16], 2X41 [17], 3ZYZ [18], 4I3G [19], 5AE6 [to be published], and 6Q7I [20]), is approximately 13 Å.

The N-glycosylation at N1 and N5 also contributes to enhance substrate binding, as the xylobiose ligand showed higher residence times inside the catalytic pocket of BxIB^{N1;5} than in BxIB^{non-glyc}. In three out of four auxiliary MD runs, xylobiose remained bound to the catalytic pocket at least twice as long in BxIB^{N1;5} (Additional file 1: Figure S4). This is attributed to the glycan chains that surround the catalytic pocket and hinder the release of the substrate.

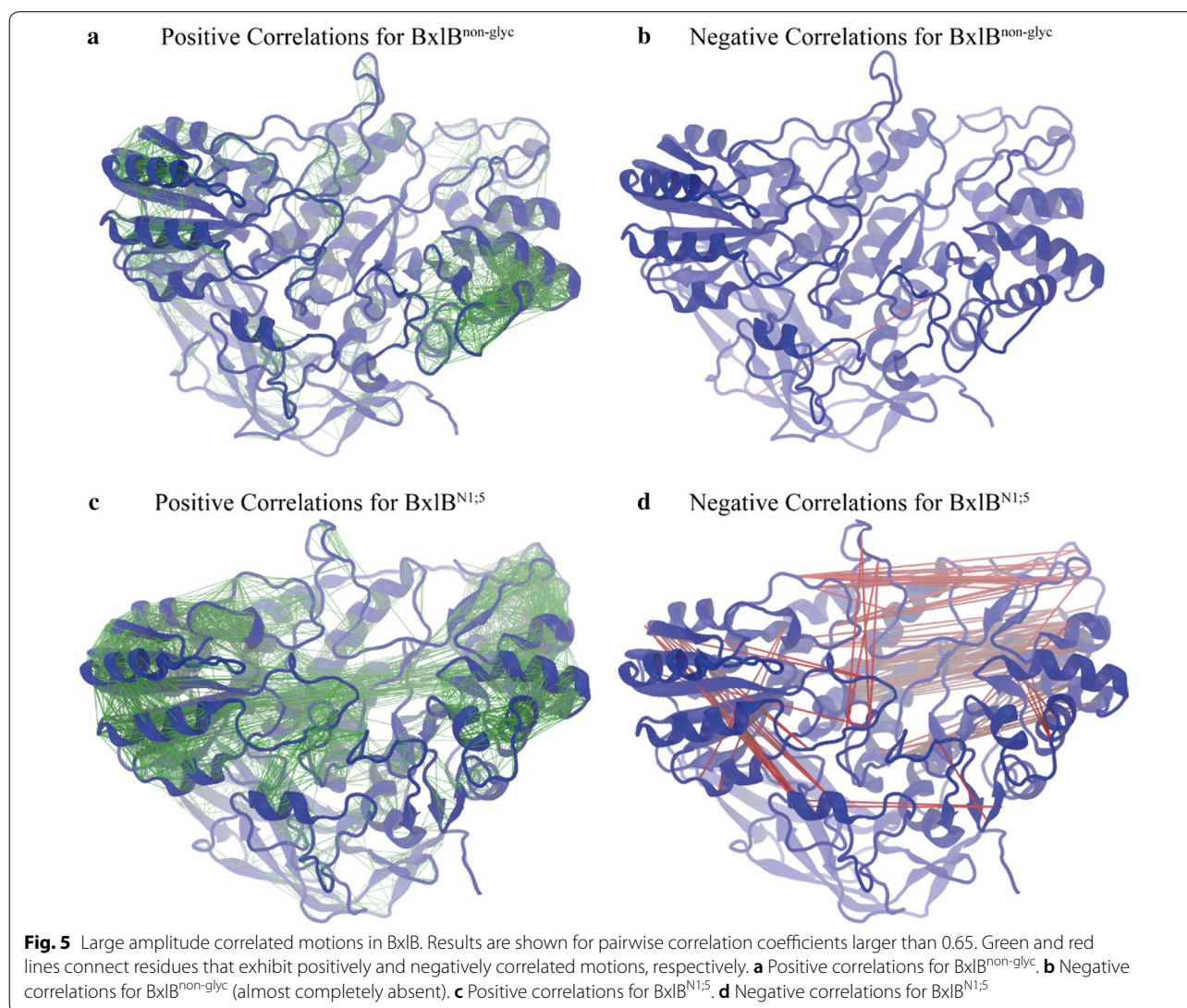
N1 and N5 glycosylation affects the pattern of large-scale motions of the enzyme

The large-amplitude, low-frequency collective motions for both BxIB^{N1;5} and BxIB^{non-glyc} were investigated via principal components analysis of the α -carbons Pearson cross-correlations using the MD trajectories [21]. Positive correlations denote pairs of residues that move

synchronously along the same direction, while negative correlations indicate pairs of residues that move synchronously along opposite directions. If two residues move independently, then the cross-correlation between them is null. BxIB^{N1;5} shows a very distinct pattern of collective motions when compared to BxIB^{non-glyc}. The glycosylation at position N1 and N5 promotes a significant increase in the overall amount of positive correlations within the structural elements of the enzyme, but also gives rise to negative correlations between spatially distant parts of the structure, which were absent in BxIB^{non-glyc} (Fig. 5).

Removal of N-glycosylation sites decreased BxIB thermal stability

Circular dichroism (CD) of the purified enzymes showed BxIB^{wt} and glycomutants to have similar secondary structure compositions, corresponding to 64% α -helix and



13% β -strand (Additional file 1: Figure S5) [22]. Nevertheless, BxlB glycomutant melting temperature range was around 8 °C, decreased from 63.8 °C for BxlB^{wt} to 61.6 °C for BxlB^{N1;5;7}, and 59.5 °C for BxlB^{non-glyc}. Six additional BxlB glycomutants also showed lower melting temperatures than the BxlB^{wt}, from 61.1 °C for BxlB^{N1;5} until 55.1 °C for BxlB^{N5;7} (Additional file 1: Table S3).

BxlB glycomutants showed lower secretion

BxlB secretion in *A. nidulans* was evaluated by Western blot (WB) using a polyclonal BxlB antibody. All the glycomutants were secreted at lower levels than that in the wild type (Fig. 6). *In silico* analyses indicated that N-glycosylation assisted BxlB^{wt} folding by encouraging a more specific route with a lower free energy barrier compared to the non-glycosylated enzyme. The curve of specific heat capacity at constant volume— C_v (Additional file 1: Figure S6) showed that, for the wild type, there was a higher peak and a wider width that can be understood as a less cooperative protein folding. Following the wild-type analysis in particular, the free energy profile (Additional file 1: Figure S7) indicated a small shoulder in the curve around $Q=0.7$, meaning that no intermediate states were being populated in the transition state, but that perturbations along the folding process may occur, similar to what happens for the other cases. Complementing both results, the ϕ -value analyses (Additional file 1: Figure S8) show for all cases that residues from the N-terminal portion (1 to 400) were involved in interactions during the transition state (TS), while the C-terminal portion (from 400 to the end of

the chain) interactions for the wild type in the TS were insignificant, indicating a more specific route where the N-terminal portion was formed earlier. The reason is the limitation imposed upon the residue angles due to the N-glycosylation that restricts the conformational space, entropically favoring the process. Analyzing the other cases, it is possible to see an increase of residues from the C-terminal portion involved in contacts in the TS proportional to the removal of N-glycosylation. Thus, during folding, the protein is conducted to intermediate states resulting in traps by the competition of contacts from both sides, increasing the free energy profiles and providing an explanation for the C_v analysis that suggests a more cooperative process (narrowest barrier).

In silico data revealed the fundamental role of N-glycans during the protein folding and highlighted how N-glycosylation engineering can be a challenge. The evaluation was mainly focused on BxlB^{wt}, BxlB^{non-glyc}, BxlB^{N1;5;7}, BxlB^{N5;7}, and BxlB^{N1} forms. The constant volume specific heat analysis (Additional file 1: Figure S6) showed a higher thermal stability for BxlB^{wt} and BxlB^{N1;5;7} when compared to BxlB^{non-glyc}, BxlB^{N5;7} and BxlB^{N1}, corroborating to the results obtained experimentally (Additional file 1: Table S3). The inset in Additional file 1: Figure S6 shows the superimposition of the curves by critical temperature (T_c) normalization. The width of the distribution indicates a slightly less cooperative folding process for BxlB^{wt}, which in this case is favorable as previously presented. This result is complemented by the analysis of the free energy profiles (Additional file 1: Figure S7) and ϕ -values (Additional file 1: Figure S8).

BxlB^{wt} presents a lower free energy barrier in the transition state (3.4 kT) when compared to BxlB^{non-glyc} (3.8 kT), correlating to faster folding according to the Arrhenius equation. Even so, the BxlB^{non-glyc} free energy profile presents an intermediate state due a less harmonious folding process by the removal of restraints (higher conformational space) imposed by the glycans (Additional file 1: Figure S7). BxlB^{wt} has more specific folding, first forming C-terminal, for then finalize the process. Furthermore, the N-glycosylations in BxlB^{wt} seem to stabilize the folded and unfolded states. Since simulations are in reduced units the results are qualitative.

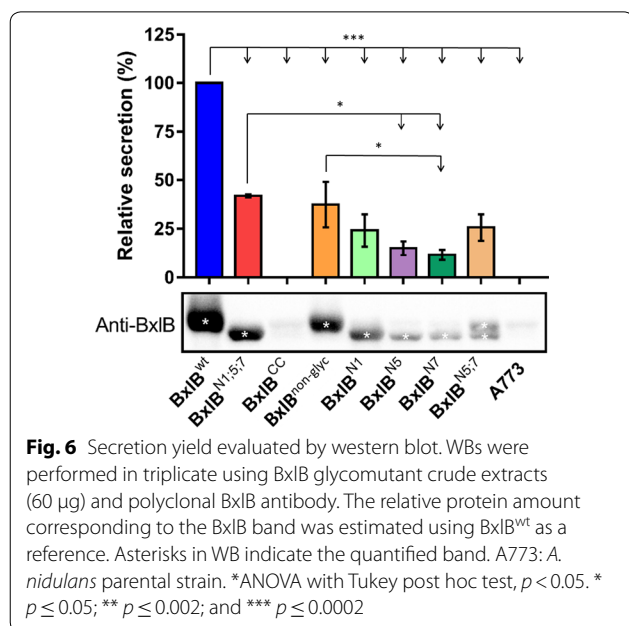


Fig. 6 Secretion yield evaluated by western blot. WBs were performed in triplicate using BxlB glycomutant crude extracts (60 μ g) and polyclonal BxlB antibody. The relative protein amount corresponding to the BxlB band was estimated using BxlB^{wt} as a reference. Asterisks in WB indicate the quantified band. A773: *A. nidulans* parental strain. *ANOVA with Tukey post hoc test, $p < 0.05$. * $p \leq 0.05$; ** $p \leq 0.002$; and *** $p \leq 0.0002$

Monitoring BxlB^{CC} secretion

The absence of detectable BxlB^{CC} secretion cannot be attributed to transcriptional impairment, as previously shown. Moreover, real-time PCR showed a non-significant difference in the transcription of *bipA* (ER chaperone) and *pdiA* (protein disulfide isomerase), genes normally associated with ER stress (data not shown) [23–25].

To further investigate the low secretion of BxIB^{CC}, we asked if the enzyme was trapped inside the cell by WB analysis. Again, BxIB^{CC} was detected at a very weak intensity (Additional file 1: Figure S9). Furthermore, BxIB^{wt} and BxIB^{CC} were detected via immunohistochemistry. The polyclonal BxIB^{wt} antibody was identified with a red fluorescence antibody by confocal microscopy (Additional file 1: Figure S10 and Additional files 2, 3, 4, 5: Videos S1–4). Strong BxIB^{wt} signals were detected in *A. nidulans* hyphae, especially in the tips, which also had a very weak BxIB^{CC} signal, corroborating the WB.

Discussion

N-glycosylation enhances BxIB folding

The *BxIB*^{wt} gene from *A. nidulans* encoding β -xylosidase was selected from a set of 265 N-glycoproteins. The high levels of β -xylosidase secretion found when *A. nidulans* was cultivated on beechwood xylan provided evidence that this enzyme was highly important for biomass degradation [4]. β -Xylosidases have been detected in various prokaryotes and eukaryotes, but, according to the mycoCLAP database [26, 27], only 11 eukaryotic GH3 β -xylosidases have been characterized. Among them, four β -xylosidases have been expressed in hosts such as *Aspergillus* spp., *Pichia pastoris*, and *Saccharomyces cerevisiae* (Additional file 1: Table S5). Here, a homologous expression system was used to prevent concerns related to accurate gene expression and protein production. In addition to the high secretion levels in the presence of lignocellulosic substrates, BxIB^{wt} can be considered a good model for studies regarding the influence of N-glycosylation on enzyme secretion and functional parameters, due to its considerable levels of N-glycosylation and enzymatic activity.

As observed in the free energy profiles (Additional file 1: Figure S7), the wild-type protein lacks an intermediate state after the transition state peak, thus showing a more specific and favorable folding process. This result is complemented by the ϕ -values analysis (Additional file 1: Figure S8) that indicates the formation of the N-terminal side of the protein preceding the folding of the C-terminal portion. The presence of an intermediate state after the transition state peak in the non-glycosylated protein's free energy profile (red line in Additional file 1: Figure S7) indicates difficulties in achieving the folded state. The ϕ -value analysis (Additional file 1: Figure S8) also indicates simultaneous folding of the N- and C-terminal portions, allowing for a less specific folding process that traps the protein in an intermediate state. The non-glycosylated state enables a higher number of accessible conformations, suggesting that for some mutations folding may not occur. N-glycans play an important role by interacting with polypeptide chains, favoring promising

folding pathways and the stabilization of the native and unfolded states. The secretion of glycoproteins is generally facilitated by their higher stability and the presence of calnexin/calreticulin quality control [28]. Furthermore, low thermodynamic stability is known to decrease protein export efficiency—i.e., very unstable proteins are poorly exported [29]. The influence of N-glycan composition on protein folding was also studied in the human immune cell receptor adhesion domain (CD2ad), and the presence of complete N-glycans was reported to provide a fourfold acceleration in folding, in addition to stabilizing the protein structure [30].

N-glycans at positions 63, 458 and 760 are important for enzyme activity

BxIB^{wt}, BxIB^{N1;5;7}, BxIB^{CC} and BxIB^{non-glyc} secretion levels were evaluated after their homologous expression in *A. nidulans*. Activity assays of the extracellular enzymes revealed that complete deglycosylation did not affect BxIB^{non-glyc} activity. On the other hand, the improvement in BxIB^{N1;5;7} enzymatic activity compared to the wild type denotes that the N-glycosylation sites at N63, N458, and N760 are important for protein folding and export. Moreover, BxIB^{CC} activity and secretion were not detected in the extracellular fraction, indicating an impairment in either gene expression, protein production, or secretion. Real-time PCR showed high transcription levels for wild type, BxIB^{N1;5;7}, BxIB^{CC}, and BxIB^{non-glyc}, suggesting that transcription is not a bottleneck for BxIB^{CC} production. There are few studies dealing with the influence of N-glycans on protein secretion, and variable results have been found. For example, changing two N-glycosylation sites (N14Q and N48Q) of a heterologous lipase expressed in *P. pastoris* did not affect its secretion, while the N60Q mutation completely abolished secretion [12]. Hence, it is possible that N-glycans attached to specific positions in the protein are essential to folding kinetics and to the secretion pathway quality control.

BxIB^{wt} deglycosylation reduces thermal stability

Secondary structure analyses of BxIB^{wt} and glycomutants revealed that all recombinant enzymes shared a classic profile, exhibiting α -helices as the predominant secondary structure (Additional file 1: Figure S5) [31]. Similarities in CD data were confirmed by deconvolution analysis, which found the same α -helix and β -strand rates (Additional file 1: Table S3). The deconvolution data were highly similar to what was found in *A. niger* β -xylosidase composed of 41% α -helix and 16% β -sheet; however, there was not as much similarity to the *T. reesei* β -xylosidase which presented 23% α -helix and 27% β -sheet composition [32, 33].

Generally, glycoproteins have higher stability than their partially glycosylated or non-glycosylated counterparts, despite the absence of structural links associated with N-glycosylation [34]. This was also observed in our study where all BxlB mutants were less stable when compared with the wild type (Additional file 1: Table S3). Recently, thermal stability was evaluated in *T. reesei* cellobiohydrolase (*TrCel7A*) by differential scanning calorimetry, with lower stability reported for all 15 N-glycosylation mutants [35]. Interactions between N-glycan sugars and amino acid residues often stabilize the protein structure; consequently, the glycosylated forms of a protein are more stable than the non-glycosylated counterpart [34, 36].

Glycosylation at N63, N458, and N760 enhances BxlB kinetic parameters

The optimal activity conditions for all BxlB glycomutants were pH 5.0 and 60 °C using ρ NP-X as substrate. The same enzyme expressed in *P. pastoris* showed optimal activity at pH 4.4 and 48 °C using rye arabinoxylin and xylohexaose as substrates [37]. This difference in reaction conditions due to N-glycosylation was also reported for β -glucosidase from *A. terreus* expressed in *P. pastoris* and *T. reesei* [13]. Kinetic parameters showed that the removal of any N-glycosylation site decreased BxlB^{wt} affinity for ρ NP-X, indicating that N-glycans may facilitate substrate recognition or affect catalytic site flexibility (*K_m* values in Table 1). Structural dynamics can influence positions and flexibility of catalytic residues, impacting kinetic parameters [38]. Wei et al. showed that removing some N-glycosylation sites decreased the specific activity of *A. terreus* β -glucosidase produced in filamentous fungi or yeast [13]. In accordance with this observation, we demonstrated that the removal of four N-glycosylation sites to form BxlB^{N1;5;7} increased *V_{max}* and *K_m*, suggesting important changes to structural dynamics.

N5 glycosylation site is essential to BxlB catalytic efficiency

Six additional mutants were designed to further understand the influence of each N-glycosylation site on folding, secretion, and BxlB^{wt} functional parameters. BxlB^{N1} secretion and catalytic efficiency decreased in comparison to BxlB^{non-glyc}. Similarly, BxlB^{N1;5;7} secretion and catalytic efficiency decreased in comparison to BxlB^{N5;7}. These data suggest that the N1 site has a slight negative influence on BxlB^{wt} kinetic parameters and secretion levels. However, for the other glycomutants that contained a single N-glycosylation site, maintaining N5 or N7 sites, showed a drastic negative influence on enzyme secretion and function. These alterations in secretion and enzyme activity were probably impacted by the N-glycan position in the 3D structure, as well as protein dynamics and stability [38, 39].

MD analysis of the catalytic site suggests that the N-glycosylation at positions N1 and N5 creates a net interaction that stabilizes the relative position of the catalytic residues, even though these two residues are not in the segments of the protein that had their flexibility mostly affected by the presence of N-glycans. That is, the suggested stabilization of the general acid/base catalytic pair may stem from the confluence of multiple long-range interactions, in which the N-glycans play a major role.

The highest activities were observed in the presence of N5 along with either N1 or N7, indicating that N5 is essential for BxlB dynamics, but is structurally stabilized by N1 or N7. As in the case of the essential N-glycosylation site in BxlB^{wt}, previous studies have also demonstrated the critical importance of a single N-glycosylation site on folding and enzymatic activity. In *P. pastoris* BglS, for instance, N224 is important for enzyme activity and production, and N428 is essential for N-acetylglucosamine-6-sulfotransferase-1 activity [13, 40]. An increased number of positive correlations throughout the enzyme structure in BxlB^{N1;5} endorses the view that glycosylation may lead to a higher number of intramolecular contacts—mainly van der Waals packing contacts [41]. As a result, the protein movements acquire more of a rigid-body quality when compared to BxlB^{non-glyc} [42, 43]. However, the N1 and N5 N-glycosylation pattern also introduced negative correlations in the BxlB structure, suggesting an important change in the pattern of the essential dynamics of the enzyme that may underlie substrate binding, product release, and the observed differences in catalytic efficiency between BxlB^{N1;5} and BxlB^{non-glyc}. Additional simulations, with different glycosylation patterns and different conditions, would be necessary to further analyze the role of N-glycans in BxlB.

Changing BxlB^{wt} N-glycosylation context impairs protein folding and secretion

Our results show that the mispositioning of N-glycosylation sites impairs the production of recombinant enzymes in *A. nidulans*. To understand the impairment of BxlB^{CC} production, microscopy experiments to monitor enzyme secretion were performed showing that BxlB^{CC} mutations affect folding and secretion. The importance of balance in translation phases has been previously reported [44]. Thus, BxlB^{CC} misfolding likely triggered protein degradation, resulting in the secretion of only a small amount of a non-functional enzyme.

Proteins with difficulty in achieving the correct folding remain longer in the ER, which maintains strict quality control, either actively facilitating folding or degrading directing misfolded proteins [28, 45]. Quality control

in *A. nidulans* is performed by the calnexin cycle. Calnexin recognizes *N*-glycans attached to proteins and assists disulfide bond formation, consequently facilitating correct folding and secretion [46, 47]. Here, confocal microscopy showed that BxIB^{CC} is retained in the intracellular fraction, suggesting that the mispositioning of *N*-glycosylation sites flagged the protein for degradation.

Conclusions

The study of the effects of *N*-glycosylation patterns on fungal CAZymes contributes to understanding how *N*-glycan positioning affects protein structure, dynamics, stability, and function. Here, we demonstrate that *N*-glycosylation facilitates the correct folding of a GH3 β -xylosidase from *A. nidulans* by eliminating an intermediate state. Despite the relatively unaffected transcriptional levels, changing the *N*-glycosylation context hampered enzyme secretion. Secondary structures were preserved in BxIB glycomutants, but thermal stabilities were reduced. While BxIB^{wt} secretion and kinetic parameters were affected by *N*-glycosylation site mutations, the non-glycosylated enzyme (BxIB^{non-glyc}) was secreted in a functional state. There is strong evidence that mispositioning BxIB *N*-glycosylation sites (BxIB^{CC}) results in unfolded/misfolded non-functional enzyme. At an individual level, the *N*-glycosylation site N5 is essential for BxIB improved enzyme catalytic efficiency, but requires additional complementation by N1 and/or N7 sites. Moreover, BxIB glycomutants demonstrate the complexity of the *N*-glycosylation effect, positively and/or negatively affecting the folding process, secretion, and kinetic parameters. *N*-glycosylation engineering is a promising tool for enhancing target enzyme secretion, activity, and thermal stability.

Materials and methods

Strains, plasmids and media

The reference strain *A. nidulans* A773 (pyrG89;wA3;pyroA4) was purchased from the Fungal Genetics Stock Center (FGSC). *A. nidulans* A773 and recombinant strains were regularly maintained in minimal media (MM): 1% glucose (m/v), pH 6.5 [11, 48]. Plasmids were propagated in *E. coli* DH5 α maintained in Luria–Bertani (LB) medium.

Site-directed mutagenesis of GH3 β -xylosidase

The *bxlB*^{wt} gene was amplified from *A. nidulans* A773 genomic DNA by PCR using specific primers (Additional file 1: Table S6). The gene was cloned into the pEXPYR shuttle vector using the NotI and XbaI sites, as previously described [11].

The following amino acid substitutions in the BxIB^{wt} sequence were designed and genes synthesized by GenOne (Rio de Janeiro, Brazil): BxIB^{N1;5;7} (N340Q, N408Q, N419Q, N621Q), BxIB^{non-glyc} (N63Q, N340Q, N408Q, N419Q, N458Q, N621Q, N760Q), and BxIB^{CC} (N63Q, A123T, Q163 N, N340Q, Q391 N, N408Q, N419Q, L450T, N458Q, N621Q, N760Q). Despite the point mutation of some amino acids in the BxIB^{CC} to potential O-glycosylation sites, none of them were predicted as glycosylated. The other six mutants, BxIB^{N1} (N340Q, N408Q, N419Q, N458Q, N621Q, N760Q), BxIB^{N5} (N63Q, N340Q, N408Q, N419Q, N621Q, N760Q), BxIB^{N7} (N63Q, N340Q, N408Q, N419Q, N458Q, N621Q), BxIB^{N1;5} (N340Q, N408Q, N419Q, N621Q, N760Q), BxIB^{N1;7} (N340Q, N408Q, N419Q, N458Q, N621Q), and BxIB^{N5;7} (N63Q, N340Q, N408Q, N419Q, N621Q) were designed using the Q5[®] Site-Directed Mutagenesis Kit (New England Biolabs).

Gene cloning and *A. nidulans* transformation

Genes cloned into the pEXPYR plasmid were transformed into calcium competent *E. coli* cells by heat shock, and confirmation was carried out using colony PCR. Positive colonies were cultivated overnight and then plasmids were extracted and used for fungal transformation.

Fungal transformation was carried out as previously described, with modifications [49]. Conidia from *A. nidulans* A773 were inoculated on YG medium (20 g·L⁻¹ glucose, 5 g·L⁻¹ yeast extract, 1 × trace elements, 1 mg·L⁻¹ pyridoxine, 2.5 mg·L⁻¹ uracil/uridine) and were incubated at 30 °C and 130 rpm for 13 h. Protoplasts were prepared by hydrolysis of the fungal cell wall with 125 mg lysozyme from chicken egg white (L7651, Sigma) and 1.02 g Vinotaste Pro (Novozymes) for 2 h. Approximately, 10 μ g of recombinant DNA was mixed with the protoplast solution and 25% PEG (w/v). Protoplast recovery was performed on MM plates supplemented with 1.2 M sorbitol and pyridoxine, incubated at 37 °C for 3 days.

LC–MS/MS validation of *N*-glycosylated sites

Purified *N*-glycomutants were incubated with 10 units of endoglycosidase-H (New England Biolabs) at 37 °C during 24 h for deglycosylation under denaturing conditions. Samples were then prepared for LC–MS/MS analysis as previously described [4]. To increase coverage and expand the number of peptide sequences, protein mutants were digested in gel with either 1 μ g trypsin (Promega) at 37 °C overnight or 1 μ g GluC (promega) at 37 °C overnight, and both simultaneously. The resulting peptides were concentrated by SpeedVac and 1 μ L of

each sample was injected for identification. Peptide loads were separated in an ACQUITY UPLC HSS T3 nano-ACQUITY Column (100 Å, 1.8 µm, 75 µm X 150 mm, Waters Corporation) in one dimension across three steps of acetonitrile (7%, 40%, 85%) over 36 min at a flow rate of 500 nL/min directly into a Synapt G2-Si mass spectrometer (Waters Corp., Milford, USA). MS/MS analyses were performed by nano-electrospray ionization in positive ion mode with a NanoLock Spray (Waters Corporation) ionization source and collected in DIA mode. The lock mass channel was sampled every 30 s. The spectrometer was calibrated with an MS/MS spectrum of [Glu1]-fibrinopeptide B human (Glu-Fib) solution (100 fmol/µL) delivered through the reference sprayer of the NanoLock Spray source.

The N-glycosylation sites were validated by N-acetylglucosamine detection on asparagine residues by adding N-acetylglucosamine (N) as a variable modification (N+203.0794) to the identification step performed by ProteinLynx Global Server (version 3.0.2; Waters Corp.). A manually created databank was used for identification with the peptide sequences of all expected protein variants. The FDR was set to 4% and was calculated using a reverse databank created on-the-fly. Relevant sequence coverage was validated within PLGS software (Additional file 6: Table S7).

Structure based models and computational analysis

Structure Based Models (SBM) [50] were employed to evaluate the folding mechanisms and stability of non-glycosylated (BxlB^{non-glyc}) and wild-type (BxlB^{wt}) enzymes. In this model, the enzyme is represented by C_α-beads and the N-glycosylations by beads in the center of mass of the saccharide rings and attached to amino acid (see details in SI). Although simple, C_α-SBM is a suitable choice since they accurately describe the folding mechanisms for several proteins [51]. The native structure (or functional tridimensional form) was constructed using Swiss Model [52], based on *A. nidulans* β-xylosidase XlnD PDB 6Q7I (45.5% identity and 62.4% similarity).

The contact map of C_α-SBM was defined by CSU-algorithm [51] and N-glycans were not considered. The simulations were carried out using the molecular dynamics software developed and tested by Whitford et al. [53]. Free energy (F) profiles and constant volume specific heat values were calculated using the weighted histogram analysis method (WHAM) [54] through simulations at various temperatures. The number of native contacts formed during the simulations (Q) was employed as a reaction coordinate to describe folding mechanisms. When Q is normalized by the total number of native contacts possible, values close to 1 indicate the *ensemble* of native conformations (nativeness).

The evaluation of how mutations interfere in the folding pathways was done by calculating φ-values, using the following equation [51, 55]:

$$\phi^i = \frac{\Delta F_{TS}^i - \Delta F_U^i}{\Delta F_N^i - \Delta F_U^i},$$

where ΔF is the free energy variation calculated by perturbation theory, i.e., evaluating the free energy difference of contacts in the presence and absence of residue *i*. These differences are related to the transition state (ΔF_{TS}), native state (ΔF_N) and unfolded state (ΔF_U). φ-values close to 1 suggest poor mutation choices, since they can destabilize the transition state or folded state, affecting the folding pathway or folding rate. In some cases, the mutation of these residues can strongly interfere with the folding process, not allowing the protein to reach its functional state. Values close to 0 suggest that mutations of these residues may not interfere in the folding process, making them good candidates for mutations, especially for protein engineering using protein-surface residues. Furthermore, the φ-value calculations help to understand folding patterns, since they show contacts formed during the transition state for each residue.

Molecular dynamics simulations

Molecular dynamics simulations were performed on the BxlB in both its N1;5 and non-glycosylated forms using the NAMD package [56] with CHARMM36 [57] force field for proteins and carbohydrates, and TIP3P water model [58]. The BxlB structure was modeled using the I-TASSER server [59], with the PDB structure 6Q7I [20] (45.5% identity and 62.4% similarity to BxlB) as a template and further refined with the GalaxyWEB server [60]. The hydrogen atoms of the enzyme were added according to the protonation state predicted by the H++ server [61, 62] at pH 5.5. The following residues were considered protonated (i.e., Asp/Glu residues electrically neutral and His residues positively charged): His67, His88, His144, Asp148, His175, His275, Asp288, His299, His300, Glu333, Glu489, Glu490, Glu510, Asp530, Glu582, Glu605, His616, and Asp649. The BxlB^{N1;5} glycosylated structure was modeled using the GLYCAM server [63], by covalently linking a Man₅GlcNAc₂ moiety to the Asn63 and Asn458 residues. Both BxlB^{N1;5} and BxlB^{non-glyc} structures were modeled with a xylobiose molecule in the active site, which was obtained from the PDB structure 5AE6 [to be published]. The simulation boxes contained, respectively to BxlB^{N1;5} and BxlB^{non-glyc}, 31,178 and 29,621 water molecules, 119 and 115 sodium ions, and 88 and 84 chloride ions. Chloride and sodium ions were added to render the system electrically neutral

at a salt concentration 0.15 mol L^{-1} . The simulations were performed using periodic boundary conditions and the particle mesh Ewald algorithm [64] with a 12 \AA cutoff and a smoothing function starting at 10 \AA . Bonds involving hydrogen atoms were constrained at their equilibrium values and the simulation time step was 2.0 fs . All simulations were performed at a constant temperature of 310 K and a constant pressure of 1 bar , using the Langevin thermostat and pressure control. After initial relaxation and thermalization, both glycosylated and non-glycosylated systems underwent a production run of 400 ns each. Three additional runs 50 ns -long were carried out with both systems to check for unbinding events.

Biochemical characterization of β -xylosidase and glycomutants

Enzymatic activity and protein determination

Fresh conidia from *A. nidulans* A773 and recombinant strains (10^7 – 10^8 per ml) were inoculated for 36 h at $37 \text{ }^\circ\text{C}$ in MM pH 6.5 supplemented with 2% (w/v) maltose. After growth, the mycelial mass was separated by filtration and the crude filtrate was centrifuged ($10,000\times g$, 20 min $4 \text{ }^\circ\text{C}$); mycelia were then washed and the intracellular content was extracted by maceration with liquid nitrogen, which was suspended in RIPA buffer and centrifuged ($10,000\times g$, 20 min $4 \text{ }^\circ\text{C}$). Protein concentration in the crude (non-purified) extracellular filtrate, as well as in the intracellular extract, was quantified by the Bradford method [65] and BCA method [66], respectively. About $20 \text{ }\mu\text{g}$ of total protein from the supernatant was run in 10% SDS-PAGE [67]. Standard β -xylosidase activity was determined in 0.05 M ammonium acetate buffer pH 5.0 at $50 \text{ }^\circ\text{C}$ using 5 mM pNP-X as a substrate. The reaction was stopped with 1 M sodium bicarbonate and the released *p*-nitrophenolate (pNP) was determined at 400 nm . One unit (U) of β -xylosidase activity was defined as the amount of enzyme releasing $1 \text{ }\mu\text{mol}$ of pNP per minute under the assay conditions.

Protein purification

All enzymes were purified by two chromatography steps using the HiPrep™ DEAE FF 16/10 column (GE Healthcare), followed by a HiLoad™ 16/600 Superdex™ 200 pg column (GE Healthcare), as previously described [14]. Purification was evaluated by SDS-PAGE and protein concentration was determined by reading absorbance at 280 nm , using the molar extinction coefficient [31] calculated from the amino acid composition (<http://web.expasy.org/protparam/>) [68].

Structural characterization by circular dichroism (CD) spectroscopy

CD analysis was carried out using a JASCO 815 spectropolarimeter (JASCO Inc., Tokyo, Japan) equipped with a Peltier temperature control unit and a 0.1 cm path length cuvette, as previously described [69]. Data from 260 to 190 nm were collected at 100 nm/min scanning speed, 1 nm spectral bandwidth, and 0.5 s response time. Melting temperatures were evaluated by spectral measurement from 20 to $100 \text{ }^\circ\text{C}$.

Effect of temperature and pH on enzyme activity

To determine the optimal temperatures of all recombinant proteins, enzyme activity was assayed as described above from 35 to $70 \text{ }^\circ\text{C}$ in 0.05 M ammonium acetate buffer, pH 5.0. Optimal pH was calculated by ranging the pH of a 0.1 M glycine–citrate–phosphate buffer from 3.0 to 12.5 at $50 \text{ }^\circ\text{C}$, using pNP-X as the substrate.

Kinetic parameters

Maximum velocity (V_{max}), Michaelis–Menten constant (K_{m}), the catalytic constant (k_{cat}), and catalytic efficiency ($k_{\text{cat}}/K_{\text{m}}$) were determined for each of the mutants using different pNP-X concentrations (1 – 20 mM). These analyses were performed at optimal conditions, 0.05 M ammonium acetate buffer, pH 5.0, and $60 \text{ }^\circ\text{C}$.

RNA extraction, transcript analysis by qPCR (quantitative real-time PCR), and primer design

Aspergillus nidulans total RNA was extracted by first grinding mycelia frozen in liquid nitrogen with a mortar and pestle, then collecting with a Direct-Zol RNA Miniprep kit (Zymo Research), according to the manufacturer's instructions. Total RNA (DNA-free) was assayed for reverse transcription using the Maxima First Strand cDNA Synthesis Kit for RT-qPCR, with dsDNase (Thermo Fisher Scientific). cDNA samples were diluted, and each qPCR reaction containing cDNA (100 ng), SYBR Green (Life Technologies), forward and reverse primers (Additional file 1: Table S6), and nuclease-free water was carried out using the ViiA™ 7 real-time PCR system (Life Technologies). All PCR reactions were performed in biological triplicate. Gene expression levels were determined using the $\Delta\Delta\text{Ct}$ method with β -tubulin (*tubC*) as the reference gene.

Confocal microscopy

Microscopic analyses were carried out by confocal microscopy based on Fischer-Parton et al. with modifications [70]. Mycelium was obtained after cultivation of *A. nidulans* strains for 24 h and 48 h , at $37 \text{ }^\circ\text{C}$ and 200 rpm in MM. The images were obtained by an LSM 510 Axiovert 200 M (Carl Zeiss) confocal inverted microscope,

fitted with an argon laser. Laser parameters were, respectively to cyan and red fluorescence, 365 and 590 nm excitation and 440 and 617 nm fluorescence emission, using the *A. nidulans* A773 strain to calibrate autofluorescence. All samples were spread over a microscope slide, *in natura*, then analyzed immediately after cultivation.

Western blot

WB analysis was carried out as described by Nutzmann et al. [71]. Total protein (60 µg) was separated by SDS-PAGE and then transferred to PVDF membrane using a wet blotting system (Bio-Rad). The membrane was blocked with 5% BSA, incubated overnight with primary antibody (BxIB) and then gently shaken at room temperature following the addition of immunoglobulin G anti-rabbit secondary antibody labeled with peroxidase. Protein detection was carried out using the Clarity Western ECL Substrate chemiluminescence detection kit (Bio-Rad), as described by the manufacturer.

Supplementary information

Supplementary information accompanies this paper at <https://doi.org/10.1186/s13068-019-1609-2>.

Additional file 1. Supplementary Tables and Figures.

Additional file 2. Video S1. BxIBwt production analysis by confocal microscopy. The polyclonal BxIB antibody was identified with a red-fluorescence antibody.

Additional file 3. Video S2. BxIBwt production analysis by confocal microscopy. The polyclonal BxIB antibody was identified with a red-fluorescence antibody.

Additional file 4. Video S3. BxIBcc production analysis by confocal microscopy. The polyclonal BxIB antibody was identified with a red-fluorescence antibody.

Additional file 5. Video S4. BxIBcc production analysis by confocal microscopy. The polyclonal BxIB antibody was identified with a red-fluorescence antibody.

Additional file 6. Table S7. LC-MS/MS analysis of BxIB glycomutants N-glycosylation sites.

Abbreviations

GHs: glycoside hydrolases; CAZymes: carbohydrate-active enzymes; GH3: glycoside hydrolase family 3; pNP-X: *p*-nitrophenyl β -D-xylopyranoside; ASA: accessible surface area; SP: signal peptide; CD: circular dichroism; MD: molecular dynamics; WB: western blot; FGSC: Fungal Genetics Stock Center; MM: minimal medium; LB: Luria-Bertani; CSU: contact of structural units; pNP: *p*-nitrophenolate; PBS: phosphate-buffered saline; SBM: structure-based models; RMSF: root mean-square fluctuations.

Acknowledgements

We thank the LNBio Mass Spectrometry staff for their assistance with LC-MS/MS and Professor Hernandes Faustino de Carvalho Laboratory for his assistance with the immunohistochemistry methodology. We would like to thank Paul Whitford for the simulation and analysis program codes. The simulations were performed at CENAPAD-SP (Centro Nacional de Processamento de Alto Desempenho em São Paulo), under the UNICAMP/FINEP-MCT project. Research was supported by LNBR-Brazilian Biorenewables National Laboratory (CNPEM/MCTIC) using the Characterization of Macromolecules

(MAC) open-access facility. The authors thank Espaço da Escrita-Pró-Reitoria de Pesquisa, UNICAMP for the language services provided.

Authors' contributions

AD conceived and designed the experiments. MVR, CRFT, FJC, MPZ, and JAG participated in the design of the study and designed, produced, purified, and characterized mutant enzymes. LCO carried out the *in silico* folding experiments. AHSD and MSS designed and carried out MD simulations. AESSG designed and carried out the qPCR and WB experiments. BJS and GHMFS carried out the LC-MS/MS experiments and analyses. MVR drafted the manuscript. CRFT, FA, AHSD, MSS, and AD revised the manuscript. All authors read and approved the final manuscript.

Funding

This research was supported by FAPESP (Grants 2012/20549-4 and 2017/22669-0 to ARLD; 2014/10068 and 2019/00098-7; and Grant 2013/08293-7 to MSS) and the Brazilian National Council for Scientific and Technological Development (CNPq) (Grants 441912/2014-1 and 304816/2017-5 to ARLD; 442352/2014-0 to LCO). MVR, CRFT, FJC and MPZ received FAPESP fellowships (13/24988-5, 16/16306-0, 17/10083-1, and 14/15403-6).

Availability of data and materials

The datasets supporting the conclusions of this article are included in the article and its additional files.

Ethics approval and consent to participate

None declared.

Consent for publication

None declared.

Competing interests

The authors declare that they have no competing interests.

Author details

¹ Department of Biochemistry and Tissue Biology, Institute of Biology, University of Campinas (UNICAMP), Rua Monteiro Lobato, 255, Cidade Universitária Zeferino Vaz, Campinas, SP 13083-862, Brazil. ² Department of Physics, Institute of Biosciences, Humanities and Exact Sciences, São Paulo State University (UNESP), São José do Rio Preto, SP 15054-000, Brazil. ³ Department of Medical Science, Faculty of Medicine, University of Campinas (UNICAMP), Campinas, SP 13083-862, Brazil. ⁴ Department of Biochemistry and Immunology, Ribeirão Preto Medical School, University of São Paulo (USP), Ribeirão Preto, SP 14049-900, Brazil. ⁵ Institute of Chemistry and Center for Computing in Engineering and Sciences, University of Campinas (UNICAMP), Campinas, SP 13084-862, Brazil.

Received: 6 March 2019 Accepted: 4 November 2019

Published online: 14 November 2019

References

- Benoit I, Culleton H, Zhou M, DiFalco M, Aguilar-Osorio G, Battaglia E, et al. Closely related fungi employ diverse enzymatic strategies to degrade plant biomass. *Biotechnol Biofuels*. 2015;8:107.
- Jordan DB, Wagschal K. Properties and applications of microbial β -D-xylosidases featuring the catalytically efficient enzyme from *Selenomonas ruminantium*. *Appl Microbiol Biotechnol*. 2010;86:1647–58.
- Larkin A, Imperiali B. The expanding horizons of asparagine-linked glycosylation. *Biochemistry*. 2011;50:4411–26.
- Rubio MV, Zubieta MP, Franco Cairo JPL, Calzado F, Paes Leme AF, Squina FM, et al. Mapping N-linked glycosylation of carbohydrate-active enzymes in the secretome of *Aspergillus nidulans* grown on lignocellulose. *Biotechnol Biofuels*. 2016;9:168.
- Weerapana E, Imperiali B. Asparagine-linked protein glycosylation: from eukaryotic to prokaryotic systems. *Glycobiology*. 2006;16:91R–101R.
- Chang X, Xu B, Bai Y, Luo H, Ma R, Shi P, et al. Role of N-linked glycosylation in the enzymatic properties of a thermophilic GH 10 xylanase from *Aspergillus fumigatus* expressed in *Pichia pastoris*. *PLoS ONE*. 2017;12:1–13.

7. Gusakov AV, Dotsenko AS, Rozhkova AM, Sinitsyn AP. N-Linked glycans are an important component of the processive machinery of cellobiohydrolases. *Biochimie*. 2017;132:102–8.
8. Shirke AN, Su A, Jones JA, Butterfoss GL, Koffas MAG, Kim JR, et al. Comparative thermal inactivation analysis of *Aspergillus oryzae* and *Thielavia terrestris* cutinase: role of glycosylation. *Biotechnol Bioeng*. 2017;114:63–73.
9. Lubertozzi D, Keasling JD. Developing *Aspergillus* as a host for heterologous expression. *Biotechnol Adv*. 2009;27:53–75.
10. Zubieta MP, Contesini FJ, Rubio MV, Gonçalves AE, Gerhardt JA, Prade RA, et al. Protein profile in *Aspergillus nidulans* recombinant strains overproducing heterologous enzymes. *Microb Biotechnol*. 2018;11:346–58.
11. Segato F, Damásio ARLL, Gonçalves TA, de Lucas RC, Squina FM, Decker SR, et al. High-yield secretion of multiple client proteins in *Aspergillus*. *Enzyme Microb Technol*. 2012;51:100–6.
12. Yang M, Yu X-W, Zheng H, Sha C, Zhao C, Qian M, et al. Role of N-linked glycosylation in the secretion and enzymatic characteristics of *Rhizopus chinensis* lipase expressed in *Pichia pastoris*. *Microb Cell Fact*. 2015;14:40.
13. Wei W, Chen L, Zou G, Wang Q, Yan X, Zhang J, et al. N-glycosylation affects the proper folding, enzymatic characteristics and production of a fungal β -glucosidase. *Biotechnol Bioeng*. 2013;110:3075–84.
14. Contesini FJ, Liberato MV, Rubio MV, Calzado F, Zubieta MP, Riaño-Pachón DM, et al. Structural and functional characterization of a highly secreted α -L-arabinofuranosidase (GH62) from *Aspergillus nidulans* grown on sugarcane bagasse. *Biochim Biophys Acta Proteins Proteomics*. 2017;1865:1758–69.
15. Qi F, Zhang W, Zhang F, Chen G, Liu W. Deciphering the effect of the different N-glycosylation sites on the secretion, activity, and stability of cellobiohydrolase I from *Trichoderma reesei*. *Appl Environ Microbiol*. 2014;80:3962–71.
16. Hrmova M, Varghese JN, De Gori R, Smith BJ, Driguez H, Fincher GB. Catalytic mechanisms and reaction intermediates along the hydrolytic pathway of a plant β -D-glucan glucohydrolase. *Structure*. 2001;9:1005–16.
17. Pozzo T, Pasten JL, Karlsson EN, Logan DT. Structural and functional analyses of β -glucosidase 3B from *Thermotoga neapolitana*: a thermostable three-domain representative of glycoside hydrolase 3. *J Mol Biol*. 2010;397:724–39.
18. Karkehabadi S, Helmich KE, Kaper T, Hansson H, Mikkelsen N-E, Gudmundsson M, et al. Biochemical characterization and crystal structures of a fungal family 3 β -glucosidase, Cel3A from *Hypocrea jecorina*. *J Biol Chem*. 2014;289:31624–37.
19. Zmudka MW, Thoden JB, Holden HM. The structure of DesR from *Streptomyces venezuelae*, a β -glucosidase involved in macrolide activation. *Protein Sci*. 2013;22:883–92.
20. Schröder SP, de Boer C, McGregor NGS, Rowland RJ, Moroz O, Blagova E, et al. Dynamic and functional profiling of xylan-degrading enzymes in *Aspergillus* Secretomes using activity-based probes. *ACS Cent Sci*. 2019;5:1067–78.
21. Amadei A, Linssen ABM, Berendsen HJC. Essential dynamics of proteins. *Proteins Struct Funct Genet*. 1993;17:412–25.
22. Louis-Jeune C, Andrade-Navarro MA, Perez-Iratxeta C. Prediction of protein secondary structure from circular dichroism using theoretically derived spectra. *Proteins Struct Funct Bioinforma*. 2012;80:374–81.
23. Heimerl K. Unfolded protein response in filamentous fungi—implications in biotechnology. *Appl Microbiol Biotechnol*. 2014;99:121–32.
24. Schröder M. Endoplasmic reticulum stress responses. *Cell Mol Life Sci*. 2008;65:862–94.
25. Sims AH, Gent ME, Lanthaler K, Dunn-Coleman NS, Oliver SG, Robson GD. Transcriptome analysis of recombinant protein secretion by *Aspergillus nidulans* and the unfolded-protein response in vivo. *Appl Environ Microbiol*. 2005;71:2737–47.
26. Strasser K, McDonnell E, Nyaga C, Wu M, Wu S, Almeida H, et al. MycoCLAP, the database for characterized lignocellulose-active proteins of fungal origin: Resource and text mining curation support. *Database*. 2015;2015:bav005.
27. Murphy C, Powlowski J, Wu M, Butler G, Tsang A. Curation of characterized glycoside hydrolases of Fungal origin. *Database*. 2011;2011:1–14.
28. Helenius A, Aebi M. Roles of N-linked glycans in the endoplasmic reticulum. *Annu Rev Biochem*. 2004;73:1019–49.
29. Wiseman RL, Powers ET, Buxbaum JN, Kelly JW, Balch WE. An adaptable standard for protein export from the endoplasmic reticulum. *Cell*. 2007;131:809–21.
30. Hanson SR, Culyba EK, Hsu T, Wong C-H, Kelly JW, Powers ET. The core trisaccharide of an N-linked glycoprotein intrinsically accelerates folding and enhances stability. *Proc Natl Acad Sci USA*. 2009;106:3131–6.
31. Kelly SM, Jess TJ, Price NC. How to study proteins by circular dichroism. *Biochim Biophys Acta*. 2005;1751:119–39.
32. Díaz-Malvárez FI, García-Almendárez BE, Hernández-Arana A, Amaro-Reyes A, Regalado-González C. Isolation and properties of β -xylosidase from *Aspergillus niger* GS1 using corn pericarp upon solid state fermentation. *Process Biochem*. Elsevier Ltd. 2013;48:1018–24.
33. Rojas AL, Fischer H, Eneiskaya EV, Kulminskaya AA, Shabalin KA, Neustroev KN, et al. Structural insights into the β -xylosidase from *Trichoderma reesei* obtained by synchrotron small-angle x-ray scattering and circular dichroism spectroscopy. *Biochemistry*. 2005;44:15578–84.
34. Imperiali B, Connor SEO. Effect of N-linked glycosylation on glycopeptide and glycoprotein structure. 1999;9:643–9.
35. Amore A, Knott BC, Supekar NT, Shajahan A, Azadi P, Zhao P, et al. Distinct roles of N- and O-glycans in cellulase activity and stability. *Proc Natl Acad Sci*. 2017;114:13667–72.
36. Shental-Bechor D, Levy Y. Effect of glycosylation on protein folding: a close look at thermodynamic stabilization. *Proc Natl Acad Sci USA*. 2008;105:8256–61.
37. Bauer S, Vasu P, Persson S, Mort AJ, Somerville CR. Development and application of a suite of polysaccharide-degrading enzymes for analyzing plant cell walls. *Proc Natl Acad Sci USA*. 2006;103:11417–22.
38. Solá RJ, Rodríguez-Martínez J, Griebenow K. Modulation of protein biophysical properties by chemical glycosylation: Biochemical insights and biomedical implications. *Cell Mol Life Sci*. 2007;64:2133–52.
39. Nagae M, Yamaguchi Y. Function and 3D structure of the N-glycans on glycoproteins. *Int J Mol Sci*. 2012;13:8398–429.
40. Desko MM, Gross DA, Kohler JJ. Effects of N-glycosylation on the activity and localization of GlcNAc-6-sulfotransferase 1. *Glycobiology*. 2009;19:1068–77.
41. Solá RJ, Griebenow K. Influence of modulated structural dynamics on the kinetics of α -chymotrypsin catalysis. *FEBS J*. 2006;273:5303–19.
42. Silveira RL, Skaf MS. Concerted motions and large-scale structural fluctuations of: *Trichoderma reesei* Cel7A cellobiohydrolase. *Phys Chem Chem Phys*. 2018;20(11):7498–507.
43. Ricci CG, Silveira RL, Rivalta I, Batista VS, Skaf MS. Allosteric Pathways in the PPAR γ -RXR α nuclear receptor complex. *Sci Rep*. 2016;6:19940.
44. Stein KC, Frydman J. The stop-and-go traffic regulating protein biogenesis: how translation kinetics controls proteostasis. *J Biol Chem*. 2019;294:2076–84.
45. Trombetta ES, Parodi AJ. Quality Control and Protein Folding in the Secretory Pathway. *Annu Rev Cell Dev Biol*. 2003;19:649–76.
46. Moremen KWK, Tiemeyer M, Nairn AWA. Vertebrate protein glycosylation: diversity, synthesis and function. *Nat Rev Mol Cell Biol*. 2012;13:448–62.
47. Schwarz F, Aebi M. Mechanisms and principles of N-linked protein glycosylation. *Curr Opin Struct Biol*. 2011;21:576–82.
48. Pontecorvo G, Roper JA, Chemmons LM, Macdonald KD, Bufton AWJ. The Genetics of *Aspergillus nidulans*. *Adv Genet*. 1953;5:141–238.
49. Szewczyk E, Nayak T, Oakley CE, Edgerton H, Xiong Y, Taheri-Talesh N, et al. Fusion PCR and gene targeting in *Aspergillus nidulans*. *Nat Protoc*. 2006;1:3111–20.
50. Clementi C, Nymeyer H, Onuchic JN. Topological and energetic factors: what determines the structural details of the transition state ensemble and “en-route” intermediates for protein folding? an investigation for small globular proteins. *J Mol Biol*. 2000;298:937–53.
51. Oliveira LC, Schug A, Onuchic JN. Geometrical features of the protein folding mechanism are a robust property of the energy landscape: a detailed investigation of several reduced models. *J Phys Chem B*. 2008;112:6131–6.
52. Waterhouse A, Bertoni M, Bienert S, Studer G, Tauriello G, Gumienny R, et al. SWISS-MODEL: homology modelling of protein structures and complexes. *Nucleic Acids Res*. 2018;46:W296–303.
53. Whitford PC, Miyashita O, Levy Y, Onuchic JN. Conformational transitions of adenylate kinase: switching by cracking. *J Mol Biol*. 2007;366:1661–71.

54. Kumar S, Rosenberg JM, Bouzida D, Swendsen RH, Kollman PA. The weighted histogram analysis method for free-energy calculations on biomolecules. I. The method. *J Comput Chem*. 1992;13:1011–21.
55. Fersht AR, Sato S. Value analysis and the nature of protein-folding transition states. *Proc Natl Acad Sci*. 2004;101:7976–81.
56. Phillips JC, Braun R, Wang W, Gumbart J, Tajkhorshid E, Villa E, et al. Scalable molecular dynamics with NAMD. *J Comput Chem*. 2005;26:1781–802.
57. Lee S, Tran A, Allsopp M, Lim JB, Hénin J, Klauda JB. CHARMM36 United atom chain model for lipids and surfactants. *J Phys Chem B*. 2014;118:547–56.
58. Jorgensen WL, Chandrasekhar J, Madura JD, Impey RW, Klein ML. Comparison of simple potential functions for simulating liquid water. *J Chem Phys*. 1983;79:926–35.
59. Roy A, Kucukural A, Zhang Y. I-TASSER: a unified platform for automated protein structure and function prediction. *Nat Protoc*. 2010;5:725–38.
60. Ko J, Park H, Heo L, Seok C. GalaxyWEB server for protein structure prediction and refinement. *Nucleic Acids Res*. 2012;40:W294–7.
61. Gordon JC, Myers JB, Folta T, Shoja V, Heath LS, Onufriev A. H++: a server for estimating pKas and adding missing hydrogens to macromolecules. *Nucleic Acids Res*. 2005;33:W368–71.
62. Myers J, Grothaus G, Narayanan S, Onufriev A. A simple clustering algorithm can be accurate enough for use in calculations of pKs in macromolecules. *Proteins Struct Funct Bioinforma*. 2006;63:928–38.
63. Woods Group (2005–2019) GLYCAM Web. Complex Carbohydrate Research Center, University of Georgia, Athens, GA. (<http://glycam.org>).
64. Darden T, York D, Pedersen L. Particle mesh Ewald: an N^{-log(N)} method for Ewald sums in large systems. *J Chem Phys*. 1993;98:10089–92.
65. Bradford MM. A rapid and sensitive method for the quantitation of microgram quantities of protein utilizing the principle of protein-dye binding. *Anal Biochem*. 1976;72:248–54.
66. Smith PK, Krohn RI, Hermanson GT, Mallia AK, Gartner FH, Provenzano MD, et al. Measurement of protein using bicinchoninic acid. *Anal Biochem*. 1985;150:76–85.
67. Laemmli UK. Cleavage of structural proteins during the assembly of the head of bacteriophage T4. *Nature*. 1970;227:680–5.
68. Gasteiger E, Hoogland C, Gattiker A, Duvaud S, Wilkins MR, Appel RD, et al. Protein identification and analysis tools on the ExPASy Server *Proteomics Protoc Handb*. Totowa: Humana Press; 2005. p. 571–607.
69. Cota J, Alvarez TM, Citadini AP, Santos CR, Neto M, Oliveira RR, et al. Mode of operation and low-resolution structure of a multi-domain and hyperthermophilic endo- β -1,3-glucanase from *Thermotoga petrophila*. *Biochem Biophys Res Commun*. 2011;406:590–4.
70. Fischer-Parton S, Parton RM, Hickey PC, Dijksterhuis J, Atkinson HA, Read ND. Confocal microscopy of FM4-64 as a tool for analysing endocytosis and vesicle trafficking in living fungal hyphae. *J Microsc*. 2000;198:246–59.
71. Nutzmans H-W, Reyes-Dominguez Y, Scherlach K, Schroeckh V, Horn F, Gacek A, et al. Bacteria-induced natural product formation in the fungus *Aspergillus nidulans* requires Saga/Ada-mediated histone acetylation. *Proc Natl Acad Sci*. 2011;108:14282–7.

Publisher's Note

Springer Nature remains neutral with regard to jurisdictional claims in published maps and institutional affiliations.

Ready to submit your research? Choose BMC and benefit from:

- fast, convenient online submission
- thorough peer review by experienced researchers in your field
- rapid publication on acceptance
- support for research data, including large and complex data types
- gold Open Access which fosters wider collaboration and increased citations
- maximum visibility for your research: over 100M website views per year

At BMC, research is always in progress.

Learn more biomedcentral.com/submissions

